공학석사학위논문

Improvement of Gold Catalyst Supported by Cerium Phosphate for Oxygen-Reduction Reaction

세륨 인산화물에 의한 금 전기화학 촉매의 산소 환원 반응 특성 향상

2013년 2월

서울대학교 대학원

재료공학부

변 수 진

Improvement of Gold Catalyst Supported by Cerium Phosphate for Oxygen-Reduction Reaction

세륨 인산화물에 의한 금 전기화학 촉매의 산소 환원 반응 특성 향상

지도교수 박 병 우

이 논문을 공학석사 학위논문으로 제출함.
2013년 2월

서울대학교 대학원
재료공학부
변 수 진

변수진의 공학석사 학위논문을 인준함.

2013년 2월

위 원 장 손 헌 준
부위원장 박 병 우
위 원 황 농 문

Abstract

The oxygen-reduction reaction was investigated on gold supported with cerium phosphate in an alkaline electrolyte. The composites with different Au/$CePO_4$ ratios were prepared by co-sputtering with varied operation powers. Two-electron reduction of oxygen to hydrogen peroxide has been found with the Au catalysts, while the Au/$CePO_4$ nanocomposite exhibited the four-electron reduction in a certain potential region. This enhancement was attributed to the electronic interactions between Au and $CePO_4$, which can be explained by shifting of Au 4*f* binding energy. Also, catalytic activity of $CePO_4$ contributed to increase the ORR activity and was confirmed by chronoamperometry.

Keywords: gold, cerium phosphate, electrocatalyst, oxygen reduction reaction, electronic effect, alkaline fuel cell, nanocomposite

Student Number: 2011-22864

Table of Contents

Appendix

List of Figures

Chapter 1.

Chapter 2.

Chapter 1. Overview

1.1. Introduction of Fuel Cells

Currently, complex devices for high performance are developed and the energy consumption is increased. Environmental issues also appear in the energy research field [1]. Therefore, new energy sources must be efficient and nature-friendly with sufficient power output and density. For these issues, various approaches are conducted using solar energy absorption, nuclear source, chemical energy conversion, etc. Among them, electrochemical conversion system is notable to substitute the preexisting combustion system. The electrochemical cell generates a voltage and current from each chemical reaction at anode and cathode electrode, and these electrochemical conversion systems are represented as several types of fuel cells.

Initially, fuel cells are based on the hydrogen oxidation (0 V vs. reversible hydrogen potential (RHE)) and the oxygen reduction reaction (1.23 V vs. RHE) with water product, as shown in Fig. 1-1. Chemical energy of hydrogen and oxygen can be converted to electrical energy by each electrochemical reaction [2]. Typically, proton-exchange-membrane (Nafion®) is used as the electrolyte for low temperature operating types. Such a membrane shows ionic-conductivity when it has enough humidity and proton ions (low pH). Overall cell reaction occurs as follows:

Anode : $2H_2 \leftrightarrow 4H^+ + 4e^-$ $E^0 = 0$ V

Cathode	: $O_2 + 4H^+ + 4e^- \leftrightarrow 2H_2O$	$E^0 = 1.23$ V
Overall reaction	: $2H_2 + O_2 \leftrightarrow 2H_2O$	$E^0 = 1.23$ V.

Oxygen cathode has an advantage in direct supply from air, despite the necessity of further activity improvement and oxygen catalyst stability [3]. However, the hydrogen fuel has an explosion probability, low energy density per volume, and difficulty in storage and transportation. Therefore, alternative fuels for anode are needed and explored, such as alcohol, small organic molecules, borohydride, etc. Among these sources, methanol is one of the most promising alternative fuels. Liquid phase of the methanol provides conveniences such as easy storage and handling, which makes the direct methanol fuel cells (DMFCs) attractive as energy conversion system. Also, the higher energy density per volume is an advantage of DMFCs [4]. The overall reactions of DMFCs are as follows:

Anode	: $CH_3OH + H_2O \leftrightarrow CO_2 + 6H^+ + 6e^-$	$E^0 = 0.05$ V
Cathode	: $3/2O_2 + 6H^+ + 6e^- \leftrightarrow 3H_2O$	$E^0 = 1.23$ V
Overall reaction	: $CH_3OH + 3/2O_2 \leftrightarrow CO_2 + 2H_2O$	$E^0 = 1.18$ V.

Alkaline systems have been studied since 1902, when Reid used an aqueous KOH electrolyte for the first alkaline fuel cell [5]. Recently, many research groups refocused alkaline polymer electrolyte fuel cells (APEFCs), instead of PEMFCs that have a number of barriers for commercialization. In alkaline media, methanol oxidation is kinetically

faster than that in acidic media and shows the higher stability for nonprecious group metal (NPGM) than acidic electrolyte [6]. The main reactions of APEFC are as follows:

Anode	: $CH_3OH + 6OH^- \leftrightarrow CO_2 + 5H_2O + 6e^-$	E^0 = -0.81 V
Cathode	: $3/2O_2 + 3H_2O \leftrightarrow 6OH^-$	E^0 = 0.40 V
Overall reaction	: $CH_3OH + 3/2O_2 \leftrightarrow CO_2 + 2H_2O$	E^0 = 1.21 V.

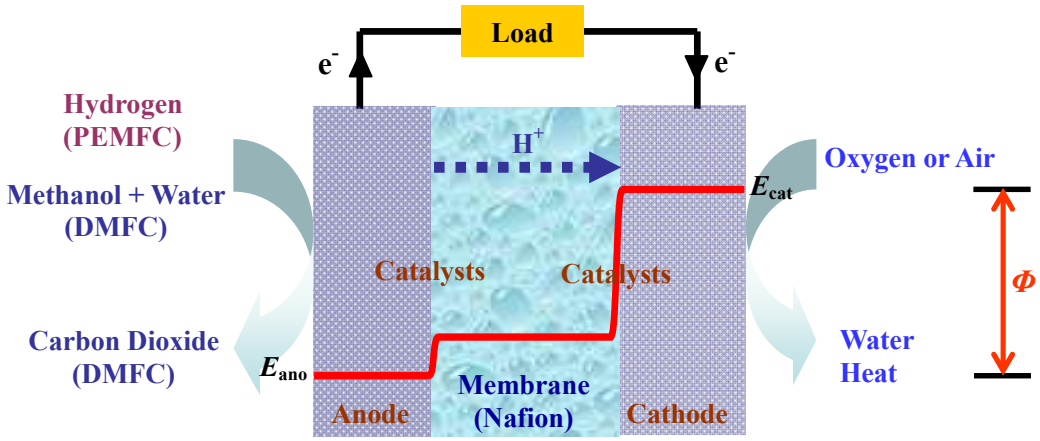

Oxidizable Chemicals		*Reducible Chemicals*
$2H_2 \leftrightarrow 4H^+ + 4e^-$ $E^0_{ano} = 0$ V (Hydrogen Oxidation)	PEMFC (1.23 V)	$O_2 + 4H^+ + 4e^- \leftrightarrow 2H_2O$ $E^0_{cat} = 1.23$ V (Oxygen Reduction)
$CH_3OH + H_2O \leftrightarrow CO_2 + 6H^+ + 6e^-$ $E^0_{ano} = 0.05$ V (Methanol Oxidation)	DMFC (1.18 V)	$3/2\ O_2 + 6H^+ + 6e^- \leftrightarrow 3H_2O$ $E^0_{cat} = 1.23$ V (Oxygen Reduction)

Fig. 1-1. (Color) Schematic figure of fuel cell with hydrogen or methanol oxidation and oxygen reduction, as the combination of anode and cathode reaction.

1.2. Fundamental of Electrocatalyst

Catalysts accelerate a rate of reaction by lowering activation energy instead of change themselves until the end of the reaction. They provide an alternative pathway for the reaction involving transition states. These properties are originated from reactant-adsorption phenomena on the catalyst surface. Catalysts can provide adsorption sites for reactants and the adsorbed reactants can be regarded as the intermediate states. The intermediate state leads to the different reaction path and the activation barrier can be reduced. Consequently, there are more collisions of reactants that have the energy needed to reach the transition state.

Effective adsorptions form a chemical bonding between an adsorbate valence level and a state of catalyst surface. It is led to the relatively strong interactions (several eV) compared to physical adsorptions due to sharing of electronic density or polarization charge transfer between adsorbate molecules and active sites of catalyst [7]. These strong electronic interactions modify the orbital of the molecules as well as the electrochemical states. Therefore, effective catalysis, such as dissociative chemical adsorptions and reaction path deviations, can occur through base interactions between orbital of objective reactant and electronic structure of catalyst surface.

Figure 1-2 is shown for change of activation barrier which depends on energy state of adsorbates. The adsorbed species have a lower energy state (*B*) and the activation barrier of adsorption is decreased (*a* to *b*) and adsorption could occur faster. In this case, activation barrier of desorption is increased, and further adsorption is

hindered with firstly adsorbed species on the active site of catalyst, thus rate of the reaction is limited, termed “rate determining step” [8]. Therefore, they may not occur nor be kinetically hindered, although reactions are thermodynamically feasible. And they may be able to promote appropriate catalyst active sites. In other words, the suitable amount of heat for adsorption is considered a key factor for the improved activity of catalyst [9].

Fig. 1-2. Change of the Gibbs energy curves for the catalytic reaction ($A + e^- \rightarrow B \rightarrow C$). The overall reaction is non-spontaneous, which needs an input of energy. *B* is intermediate state adsorbed on the catalyst surface, and Gibbs energy decreases from state (1) to (2). The activation barriers for two situations are also decreased from (a) to (b), and easier chemisorption may accelerate the reaction [8].

1.3. Mechanism of Oxygen Reduction

The reduction of oxygen is one of the most important reactions in determining the efficiency of fuel cells. As discussed in 1.1, oxygen reduction reaction on cathode has the thermodynamic potential of 1.23 V (vs. RHE at standard conditions). However, in practice, the expected potential is never achieved. Most of the efficiency losses are caused by mass transfer resistance and charge transfer resistance at the cathode interface, and the resistances make a large over potential that leads to a slow reaction onset [12]. Therefore, decreasing cathodic over potential is vitally important to overcome the low efficiency problem and make low-temperature fuel cells.

A number of reaction mechanisms for oxygen reduction have been proposed, but there are still undiscovered parts which are too complicated to be investigated as shown in Fig. 1-4. But oxygen reduction proceeds predominantly in two different pathways which are "series" 4-electron reduction and "direct" 4-electron reduction pathways. The former serial reaction is based on hydrogen peroxide as the intermediate and the latter direct reaction reduces oxygen directly to water or hydroxyl ion as a product. In alkaline media, these two main pathways for the ORR are [10]:

$$O_2 + 2H_2O + 4e^- \leftrightarrow 4OH^- \qquad E^0 = 0.402 \text{ V (vs. RHE)} \qquad (1)$$

$$O_2 + H_2O + 2e^- \leftrightarrow HO_2^- + OH^- \qquad E^0 = -0.065 \text{ V (vs. RHE)} \qquad (2a)$$

$$HO_2^- + H_2O + 2e^- \leftrightarrow 3OH^- \qquad E^0 = -0.867 \text{ V (vs. RHE)} \qquad (2b)$$

In the “series” 4-electron pathway, the major intermediate state hydrogen peroxide (HO_2^-) can be further reduced to hydroxyl ion (OH^-) with additional 2 electrons (eq. 2a, 2b) or can be diffused out to electrolyte (eq. 2a). The reason for different reaction mechanism is the absorption shape of O_2 molecules which is determined by the catalyst surface. Dissociative adsorption on catalyst can reduce oxygen completely and form OH^- (eq. 2a, 2b). In case of associative adsorption, reduction finishes at the HO_2^- (eq. 2a) that leads to half of limiting current density compared with dissociative adsorption. Thus, it can be concluded that the oxygen bonding shape is so sensitive to catalyst surface that the pathways depend on the crystallographic orientation. Then they effect to total limiting current of ORR.

Fig. 1-3. Pathways of oxygen reduction in alkaline electrolyte. The subscripts sa, a, b, and * represent strong absorption, weak absorption, bulk, and environs of catalyst, respectively [11].

1.4. Electrocatalysts for Oxygen Reduction Reaction

The different electronic interactions between oxygen (O) and various metal catalysts (M) lead to diverse O-M adsorption binding energies, and intermediate states are determined by those differences. The ORR proceeds through the intermediate states. Many researchers have already suggested this tendency is represented with volcano shaped plot for ORR as shown in Fig. 1-4 [12]. Pt and Pt-based catalysts are the most common and best electrocatalysts for ORR. It is found that oxygen is bound suitably on Pt surface with coupling orbitals of O_2 and Pt [7, 12], which can be explained by the intermediate states and the fast kinetics of oxygen reduction. In this orbital coupling, electron densities of the Pt-O bond are increased and that of O-O double bond are decreased. It means that dissociation adsorption of oxygen proceeds on Pt. Each dissociated oxygen atom forms water with neighboring protons in acidic media or forms hydroxyl ions in alkaline media. The water molecules or hydroxyl ions are detached from Pt surface and diffuse out to electrolyte. A lot of research of ORR on Pt has been undertaken and discovered an efficient pathway is required the dissociation of O-O double bonds, which is corresponding the direct 4-electron pathway [13].

Adzic's group showed correlation between oxygen reduction activities and *d*-band center energies [14]. Volcano-type relation was revealed from the calculation, as shown in Fig. 1-4. They classified transition metals into three types according to position of *d*-band center. Firstly, metals with high-lying *d*-band centers, such as Pd, Ph, Ir and Ru, can absorb oxygen intensely. The adsorption makes O-O double bond break

easily, but adsorption of oxygen (O-M) is too strong to be desorbed from active site. Reactants approaching subsequently are hard to adsorb due to oxygen atoms covering active sites. In contrast, metals that have low-lying ε_d, for example Au and Ag, bind oxygen with lower strength. At this orbital coupling, electron densities of the O-M bond are slightly increased simultaneously with slightly decreasing densities of O-O double bond. Therefore, oxygen molecules cannot dissociate on catalyst surface, most of O-O bonds are just reduced to hydrogen peroxide as product through the 2-electron pathway. Contrastively, Pt has *d*-band centers for suitable adsorption strength that O-M adsorption is neither too weak nor too strong. Dissociative adsorption and easy desorption of the adsorbed oxygen atoms on the Pt lead to 4-electron reduction pathway. This relation is plotted in Fig. 1-4. In other words, balance between adsorption and desorption is important factor for the oxygen reduction, and the balance is changed by variation of catalyst-electronic states.

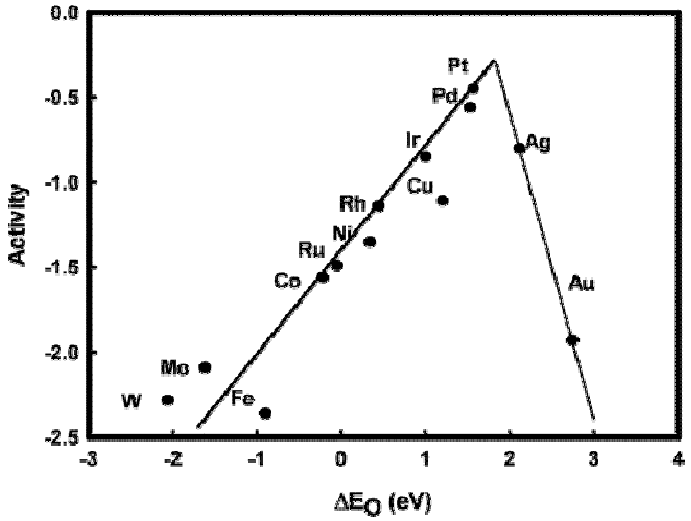

Fig. 1-4. Trends of ORR activity on various metal catalysts as a function of the oxygen binding energy (ΔE_O). Using density functional theory (DFT) calculations, many research groups discovered that oxygen adsorption energy and reduction activity have a volcano type relationship [12].

Fig. 1-5. Kinetic currents of ORR on the various metals in 0.1 M NaOH solution as a function of the metal *d*-band centers. The y-axis value, (ε_d - ε_F), is relative *d*-band center energy to the Fermi energy level [14].

1.5. Improvement of Catalytic Activity

As the interest for catalysts with low platinum content grows, the research about the effective factors on catalytic activity is expanding, although it is hard to divide the factors that influence catalytic activity simultaneously. Recently, a lot of challenges controlling the factors have achieved to redesign catalysts.

As discussed above, researchers are focusing the relation of reactant-adsorption strength with catalytic activity and finding suitable bonding energy (O-M) at the non-Pt catalysts. They use charge unbalance between catalyst and another support material. The modified electronic structure of the catalyst can influence the oxygen reduction paths, which is called electronic effect. In this point of view, Au catalysts are modified for enhancing ORR by combined several oxide materials such as defective MgO [15] and reducible oxides TiO_2 [16]. As shown in Fig. 1-6, adjacent defects of oxide material effect on Au catalyst with the transfer of electron density. The transfer of electrons leads the change in the electronic structure of Au then catalytic activity can be modified, which is an application of electronic effect on catalyst.

There is also synergetic effect from the combination of different catalysts. Further reduction or oxidation appears not on active catalyst but on another support material acting as a catalyst. Electrochemical results, such as CVs of the combination catalyst, show synergetic effect that may contribute to increase limiting current and lower overpotential. The binary catalyst is regarded as a useful and powerful strategy for design of catalysts. Achieving the synergetic effects between noble metal and

inexpensive metal oxide, such as Ag/MgO_x [17] and Au/SnO_x [18] is studied. In addition, noble metal nanoparticles supported on metal oxide or metal phosphate have been reported as improved catalysts. Geometric effect is also considered at the interface where adsorptions favor matching the lattice of catalyst and atomic distance of reactants.

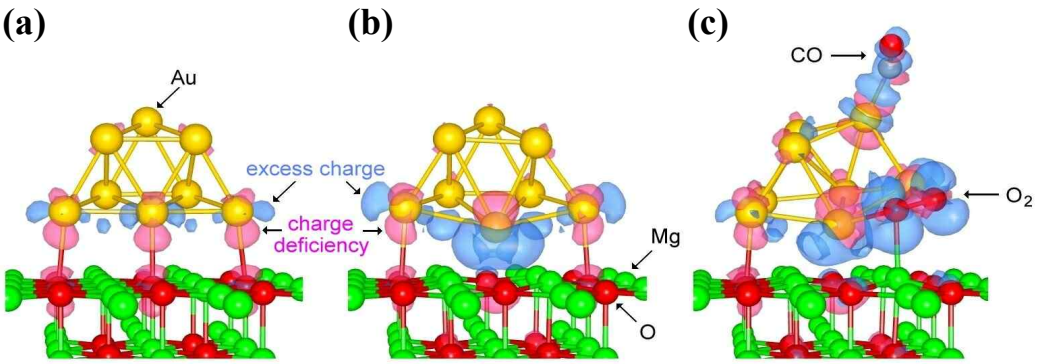

Fig. 1-6. (Color) Charge distribution of gold cluster on (a) a perfect MgO surface, (b) oxygen deficient MgO surface, and (c) redistribution of charge by adsorbing reactants [15].

1.6. References

1. K. V. Kordesch and G. R. Simader, "Environmental Impact of Fuel Cell Technology," *Chem. Rev.* **95**, 191 (1995).
2. J. M. J. Blomen and M. N. Mugerwa, *Fuel Cell Systems*, Plenum Press, 1993.
3. J. Larminie and A. Dicks, *Fuel Cell Systems Explained*, John Wiley & Sons, 2000.
4. L. Carrette, K. A. Friedrich, and U. Stimming, "Fuel Cells - Fundamentals and Applications," *Fuel Cells* **1**, 5 (2001).
5. E. H. Yu and K. Scott, "Development of direct methanol alkaline fuel cells using anion exchange membranes," *J. Power Sources* **137**, 248 (2004).
6. A. V. Tripkovic, K. D. Popovic, B. N. Grgur, B. Blizanac, P. N. Ross, and N. M. Markovic, "Methanol electrooxidation on supported Pt and PtRu catalysts in acid and alkaline solutions," *Electrochim. Acta* **47**, 3707 (2002).
7. B. Hammer and J. K. Norskov, "Theoretical Surface Science and catalysis," *Adv. Catal.* **45**, 71 (2000).
8. W. Vielstich, A. Lamm, and H. A. Gasteiger, *Handbook of Fuel Cells - Fundamentals Technology and Applications*, John Wiley & Sons, 2003.
9. J. K. Norskov, T. Bligaard, A. Logadottir, J. R. Kitchin, J. G. Chen, S. Pandelov, and U. Stimming, "Trends in the Exchange Current for Hydrogen Evolution," *J. Electrochem. Soc.* **152**, J23 (2005).
10. J. Kim and A. A. Gewirth, "Mechanism of Oxygen Electroreduction on Gold Surfaces in Basic Media," *J. Phys. Chem. B* **110**, 6 (2006).

11. S. Strbac and R. R. Adzic, "The Influence of OH^- Chemisorption on the Catalytic Properties of Gold Single Crystal Surfaces for Oxygen Reduction in Alkaline Solutions," *J. Electroanal. Chem.* **403**, 169 (1996).

12. J. K. Norskov, J. Rossmeisl, A. Logadottir, and L. Lindqvist, "Origin of the Overpotential for Oxygen Reduction at a Fuel-Cell Cathode," *J. Phys. Chem. B* **108**, 17886 (2004).

13. S. Yotsuhashi, Y. Yamada, T. Kishi, W. A. Diño, H. Nakanishi and H. Kasai, "Dissociative Adsorption of O_2 on Pt and Au Surfaces: Potential-Energy Surfaces and Electronic States," *Phys. Rev. B* **77**, 115413 (2008).

14. F. H. B. Lima, J. Zhang, M. H. Shao, K. Sasaki, M. B. Vukmirovic, E. A. Ticianelli, and R. R. Adzic, "Catalytic Activity-*d*-Band Center Correlation for the O_2 Reduction Reaction on Platinum in Alkaline Solutions," *J. Phys. Chem. C* **111**, 404 (2007).

15. B. Yoon, H. Häkkinen, U. Landman, A. S. Wörz, J.-M. Antonietti, S. Abbet, K. Judai, and U. Heiz, "Charging Effects on Bonding and Catalyzed Oxidation of CO on Au_8 Clusters on MgO," *Science* **307**, 403 (2005).

16. Z. Jiang, W. Zhang, L. Jin, X. Yang, F. Xu, J. Zhu, and W. Huang, "Direct XPS Evidence for Charge Transfer from a Reduced Rutile TiO_2(110) Surface to Au Clusters," *J. Phys. Chem. C* **111**, 33 (2007).

17. D. A. Slanac, A. Lie, J. A. Paulson, K. J. Stevenson, and K. P. Johnston, "Bifunctional Catalysts for Alkaline Oxygen Reduction Reaction via Promotion of Ligand and Ensemble Effects at Ag/MnO_x Nanodomains," *J. Phys. Chem. C* **116**,

11032 (2012).

18. D. S. Gatewood, D. E. Ramaker, K. Sasaki, and K. E. Swider-Lyonsa, “Support Effects on Water Activation and Oxygen Reduction over Au/SnO_x Electrocatalysts Observed with X-Ray Absorption Spectroscopy,” *J. Electrochem. Soc.* **155**, B834 (2008).

Chapter 2. Improvement of Gold Catalyst Supported by Cerium Phosphate for Oxygen-Reduction Reaction

2.1 Introduction

2.1.1. Non-Pt Electrocatalyst and Oxygen Reduction on Au

Fuel cells have attracted a lot of interest as devices for converting chemical energy to electrical energy. They are considered as one of the key technologies for green economy. However, a large cathodic overpotential caused by slow kinetics of oxygen reduction has been a major problem in fuel cell technology, which leads to a low conversion efficiency [1]. Even though Pt-based catalysts are currently preferred as electrocatalyst for the oxygen reduction, the high cost of the Pt is a barrier for commercialization. For these reasons, it has arisen that the need of redesigning a catalysts with high catalytic performance and low noble metal portion [2]. It has been demonstrated that binary catalyst systems are effective strategy among the various approaches [3,4].

The ORR pathway needs to be further investigated. However, oxygen reduction proceeds predominantly in two different pathways, which are “direct” 4-electron reduction and “series” 4-electron reduction pathways. The former direct reaction reduces oxygen directly to water or hydroxyl ion as products, and the latter serial reaction is based on hydrogen peroxide as the intermediate state. In alkaline media, these two main pathways are expressed as follows [5]:

$$O_2 + 2H_2O + 4e^- \leftrightarrow 4OH^- \qquad E^0 = 0.402 \text{ V (vs. RHE)} \quad (1)$$

$$O_2 + H_2O + 2e^- \leftrightarrow HO_2^- + OH^- \qquad E^0 = -0.065 \text{ V (vs. RHE)} \quad (2a)$$

$$HO_2^- + H_2O + 2e^- \leftrightarrow 3OH^- \qquad E^0 = -0.867 \text{ V (vs. RHE)} \quad (2b)$$

The pathways are sensitive to the crystallographic orientation on gold. The "direct" 4-electron pathway can be observed mainly on the Au (100) (eq. 1), while Au (110) and Au (111) show just 2-electron reduction in which hydrogen peroxide (HO_2^-) diffuses out to electrolyte (eq. 2a) [6]. The 2-electron reduction was also observed in polycrystalline Au, because Au (111) is abundant due to its lowest surface energy of close packing structure.

In this research, the Au/$CePO_4$ binary catalysts were obtained with different atomic ratios of Au and $CePO_4$. We examined the catalytic activity of pure Au and the Au/$CePO_4$ nanocomposites for oxygen-reduction reaction (ORR) in alkaline solution. It was presented not only the enhancement of limiting current but also the decreased overpotential. The role of $CePO_4$ from synergetic effect on the Au/$CePO_4$ nanocomposite was studied. Moreover, the optimum atomic ratio of Au/$CePO_4$ nanocomposite for ORR was found.

2.2 Experimental Section

The Au/$CePO_4$ nanocomposites were deposited on ITO coated glass by rf magnetron sputtering with Au and $CePO_4$ targets. The deposition was performed with various operation powers for different Au/$CePO_4$ compositions at room temperature under Ar atmosphere. The Au/$CePO_4$ nanocomposites were annealed at 200°C for 30 min under vacuum for better adhesion onto the ITO electrodes. To compare the ORR activities, pure Au, pure Pt, and $CePO_4$ electrodes were also prepared.

Electrochemical characterizations were performed using a potentiostat (CHI 604A: CH Instrumental Inc.). Hg/HgO (0.098 V vs. RHE) and Pt wire were used as the reference and counter electrode. Oxygen reduction was measured in an O_2-saturated 0.1 M NaOH solution with fixed 30 sccm oxygen flow, and H_2O_2 reduction measurement was carried out in a N_2-purged 0.1 M NaOH solution with 1.2 mM hydrogen peroxide (3 wt. % in H_2O). The electrochemical surface area (ESA) was estimated by an underpotential deposition (UPD) of lead with 1 mM lead nitrate ($Pb(NO_3)_2 \cdot 3H_2O$: Sigma-Aldrich) dissolved in 0.1 M NaOH solution. Total charge of desorption peaks was investigated to measure ESA value of gold catalyst. The potentials of desorption peaks were also used as the indication of Au surface facets. X-ray photoelectron spectroscopy (XPS, Sigma Probe: Thermo VG Scientific) was used to analyze the electronic states of Au with monochromatic Al *Kα* radiation. The binding energy scale was calibrated with C 1*s* peak at 284.6 eV. The grain sizes of Au were determined by x-ray diffraction (XRD, New D8 Advance: Bruker) and estimated by the

Scherrer equation. An inductively coupled plasma-atomic emission spectrometer (ICP-AES, Optima-4300 DV: Perkin-Elmer) was operated to measure the atomic ratio of Au/Ce in the Au/$CePO_4$ nanocomposites.

2.3 Results and Discussion

2.3.1. Gold Surface Structure and Active Surface Areas

As discussed above, ORR on gold surface occurs through different pathways depending on the surface structure. Among the low index planes, Au (100) exhibits the highest activity through the "series" 4-electron reduction pathway (eq. 2a, 2b) [7], whereas partial oxygen reduction to hydrogen peroxide (eq. 2a) is found on the Au (111) and Au (110) [8]. As shown in Fig. 2-1, lead under potential deposition (UPD) was conducted to characterize the surfaces of the Au/$CePO_4$ nanocomposites before estimation of the ORR activities. The peak potentials of UPD profile exhibit distinct indications with respect to the orientation of the gold surface. The desorption-peak potentials, 0.435, 0.56, and 0.475 V indicate Au (111), (110), and (100), respectively and marked with dotted lines in Fig. 2-1 [9]. By comparing the obtained UPD profiles with those of single orientations, it was revealed that the samples mainly consisted of Au (111) and Au (110) with similar proportions by the two main Pb^{2+} desorption peaks. From the results of UPD profiles, partial oxygen reduction (eq. 2a) generating HO_2^- intermediate state could be expected.

The electrochemical surface areas (ESAs) of Au, also, were calculated from the charge of desorption peaks. The ESAs were proportional to the charge of desorption, and the values were 1.91, 1.77, 2.28, and 1.60 (cm^2 per cm^2 sample) for pure Au, Au/Ce = 23.75, 18.81, and 11.55 nanocomposites, respectively. The surface area of the Au/Ce = 18.81 composite was the highest value.

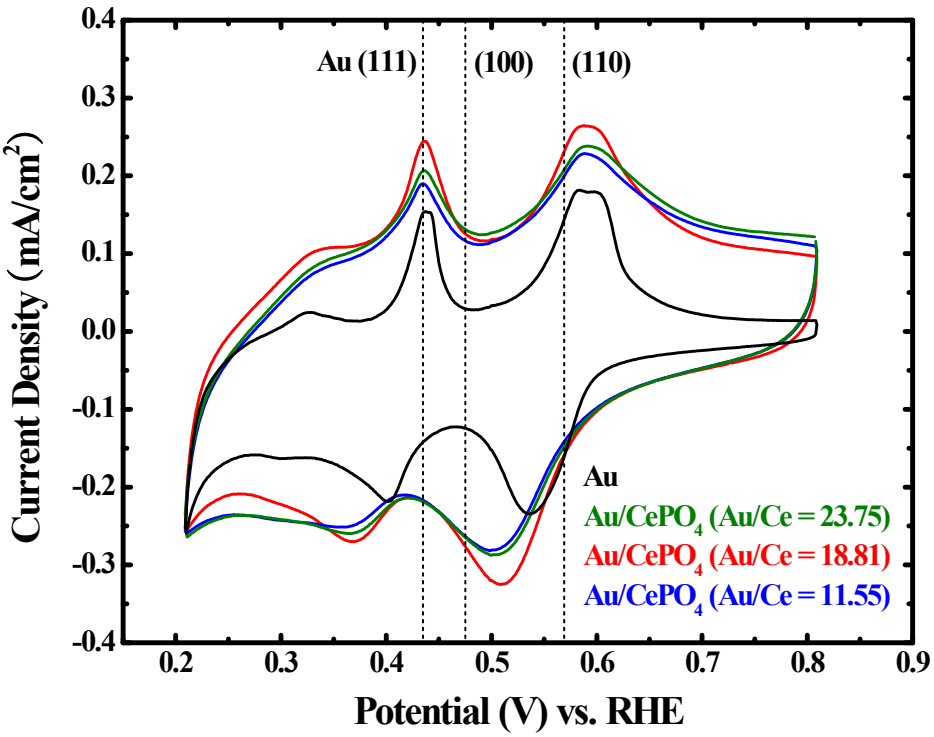

Fig. 2-1. (Color) Voltammetric profiles of the Au and the $Au/CePO_4$ nanocomposites in a N_2-purged lead nitrate solution (1 mM $Pb(NO_3)_2$ dissolved in 0.1 M NaOH solution) at a scan rate of 50 mV/s. The two main desorption peaks indicate gold surface facet (111) and (110), respectively.

2.3.2. Oxygen Reduction Reaction of Nanocomposites

To compare the oxygen reduction activities of the Au and the Au/$CePO_4$ composites, cyclic voltammograms were obtained in an O_2-saturated 0.1 M NaOH solution, as shown in Fig. 2-2. By co-sputtering $CePO_4$ with Au, the limiting current increases by a factor of 2 within the potential region of approximately 0.9 - 0.55 V, and the onset potential shifts to positive direction, up to ~50 mV. Among the nanocomposites, the Au/$CePO_4$ nanocomposite with Au/Ce = 18.81 exhibits the most enhanced catalytic properties for oxygen reduction. The current density of the Au/Ce = 18.81 sample is comparable to that of pure Pt, which is nearly twofold value of pure Au.

The limiting current density, i_L, can be calculated from the formula as follows: $i_L = -DnFc^*/\delta$ [10], where D is O_2 diffusion coefficient (2.6×10^{-5} cm^2/s) [11], F is Faraday constant (96,485 C/mol), c^* is O_2 bulk concentration (1.26 mM) [16], n is the number of involved electrons, and δ is the diffusion layer thickness (200 μm), assuming there is no convection [12]. The limiting current densities were evaluated approximately as -0.32 mA/cm^2 and -0.63 mA/cm^2, where n was 2 and 4, respectively. The values indicate the oxygen is mainly reduced through 2-electron process on the pure Au, which was expected from UPD data verifying the surface orientation. They also present that the Au/$CePO_4$ nanocomposite of optimum ratio undergoes 4-electron process. From these results, we suggest that the complete reduction of oxygen occurs at the nanocomposite with optimum ratio of Au/$CePO_4$ and its kinetic activity is enhanced.

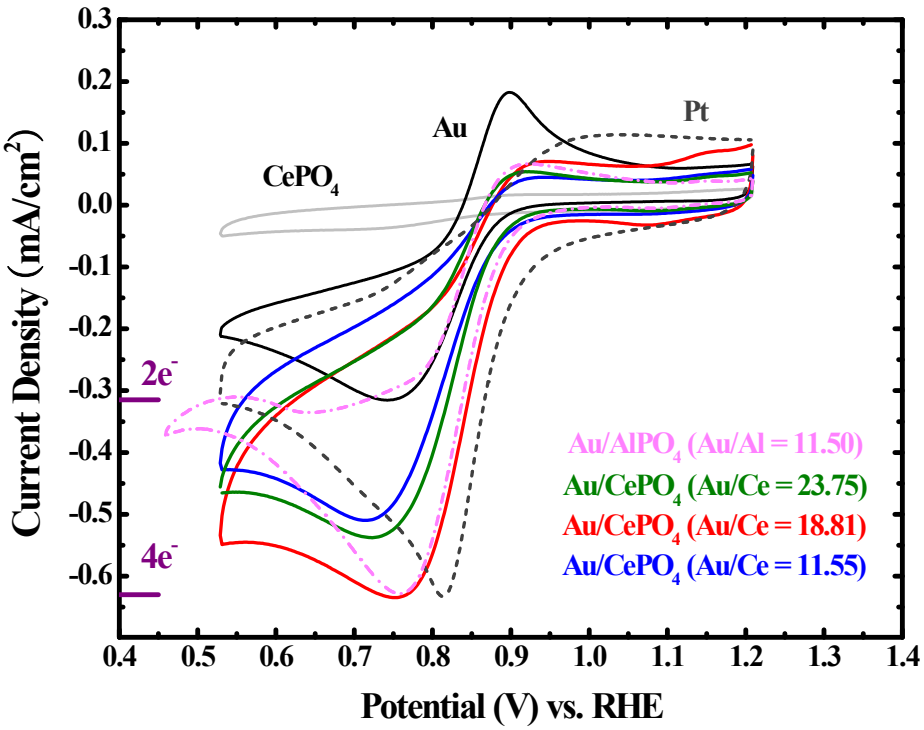

Fig. 2-2. (Color) Cyclic voltammetry curves of oxygen reduction for Au, $CePO_4$, the $Au/AlPO_4$ nanocomposite and the $Au/CePO_4$ nanocomposites recorded in an O_2-saturated 0.1 M NaOH solution with a scan rate of 50 mV/s. Also, the ORR of $Au/AlPO_4$ nanocomposite was measured.

2.3.3. Electronic Interactions between Au and $CePO_4$

Figure 2-3 shows the XPS spectra of Au 4*f* region with the various Au/$CePO_4$ ratios. Pure Au is identified by two peaks for Au $4f_{5/2}$ and Au $4f_{7/2}$ of 87.7 and 84.0 eV, respectively. In the case of Au/$CePO_4$ nanocomposites, the Au binding energies shift toward lower energy with increasing ratio of $CePO_4$, and the Au $4f_{7/2}$ reaches 83.38 eV at the ratio Au/Ce = 18.81. The ratio that shows most negative charge is consistent with ORR optimum ratio, demonstrating the electronic structure of catalyst has an effect on catalytic activity. This modified electronic structure of Au is due to the electron transfer from $CePO_4$ to Au. Although we observed charge transfer from Au 4*f* level, many researchers have shown that the shift direction of core level B.E. is in accordance with that of valence level [13]. Therefore, the effect of charge transfer on valence states also can be examined by 4*f* level shift using XPS measurements.

By the charge transfer from $CePO_4$ to Au, Au *d*-band center (ε_d) is shifted up toward Fermi level (ε_F), and the antibonding states also appear above the Fermi level. As the number of the unfilled antibonding states increases, the chemisorptions between O_2 and Au get stronger [14]. The stronger bonding (Au-O) leads to the transition of oxygen adsorption model from association to dissociation by breaking double bond between oxygen atoms. Therefore, the experimental results of "4-electron reduction" in Fig. 2-2 can be explained by this dissociative adsorption on the Au/$CePO_4$ nanocomposite. As a result, catalytic activity of Au was modified by charge movement from support material, $CePO_4$, and this is called "Electronic effect".

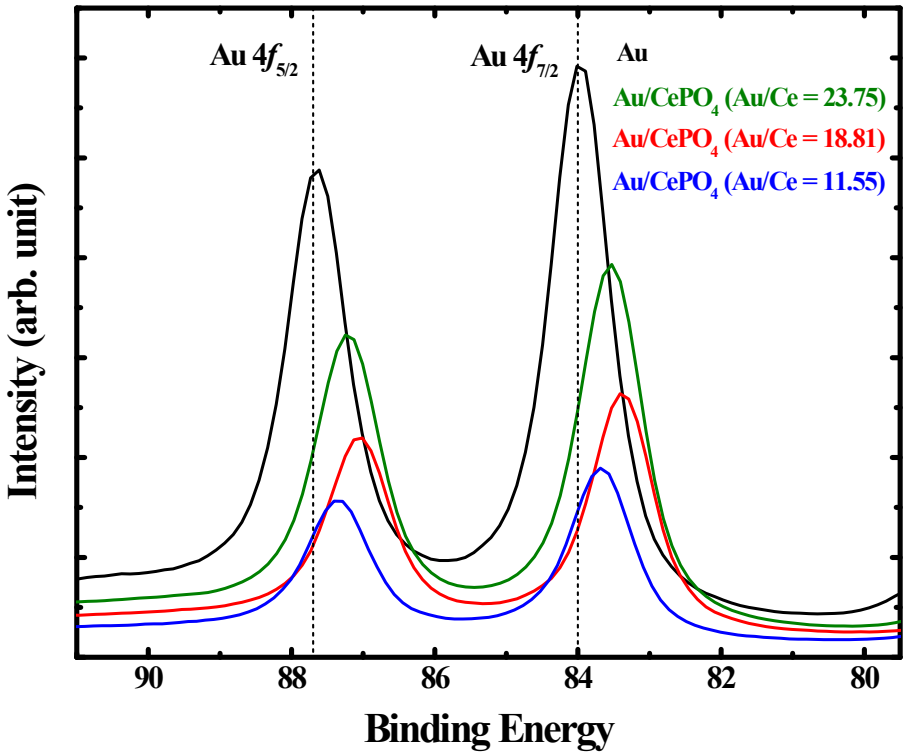

Fig. 2-3. (Color) Au 4*f* XPS spectra for the Au and the Au/$CePO_4$ nanocomposites. The dashed lines are from the standard sample of Au. The Au binding energies shift to the lower energy with increasing power of $CePO_4$ sputtering.

2.3.4. Catalytic Behaviors of $CePO_4$: Reduction of Hydrogen Peroxide

Figure 2-4 shows the chronoamperomety for Au, $CePO_4$, $AlPO_4$ and the Au/$CePO_4$ nanocomposites. The applied potential of chronoamperometry was chosen from diffusion controlled potential region of ORR, range below 0.73 V from Fig. 2-2. Then H_2O_2 was added to a N_2-purged 0.1 M NaOH solution. Even though the HO_2^- reduction is rarely observed on pure Au, and $CePO_4$ shows no catalytic property as shown in Fig. 2-4(a), the reduction peak of Au/$CePO_4$ composites at the fixed potential (0.709V) was observed immediately after injection of HO_2^-. The nanocomposite with the atomic ratio of 18.81 was the most active catalyst and the phenomenon is interpreted as a synergetic interaction.

As shown in Fig. 2-4(b), the H_2O_2 was added to pure $CePO_4$ in order to understand a role of pure $CePO_4$ intuitively. Observable reduction current occurred and the reduction peak increased as applied potential became negative, down to 0.509 V. This result can be interpreted as $CePO_4$ has its own catalytic effect for HO_2^-. Surprisingly, no activity was appeared at 0.709 V, which is enough potential for oxygen reduction. In previous work of our group, Au/$AlPO_4$ nanocomposite was proposed as a catalyst which shows the enhanced oxygen reduction activities [15]. However, the performance of pure $AlPO_4$ about H_2O_2 was undiscovered. In this paper, the chronoamperomety was performed on $AlPO_4$ under the same condition, and it could provide an explicit explanation that $AlPO_4$ has no activity with H_2O_2, as shown in Fig. 2-4(c).

This distinguishable feature between $CePO_4$ and $AlPO_4$ also could be confirmed by the different shape of cathodic peak from Fig.2-2. Under voltage range from 0.709 V to 0.529 V, the reduction current of $Au/CePO_4$ was maintained compared to that of $Au/AlPO_4$ and Pt which shows decreasing tendency. Based on the results, it is suggested that reduction of residual HO_2^- from uncompleted ORR is possible on the $CePO_4$ [13].

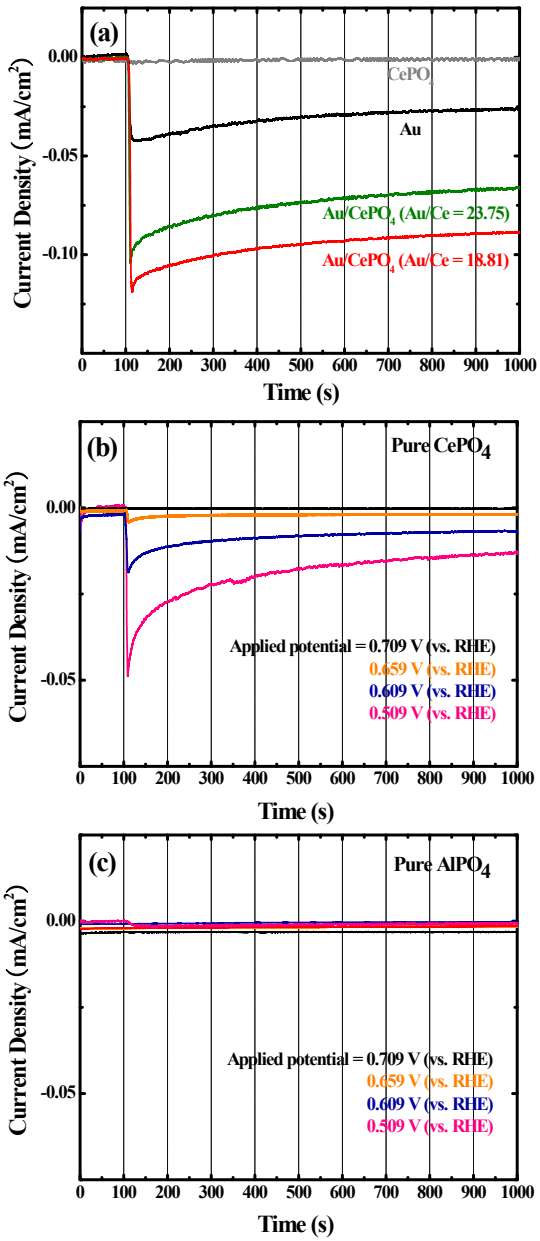

Fig. 2-4. (Color) Chronoamperometry in a N_2-purged 0.1 M NaOH solution, adding 1.2 mM H_2O_2 after 100 seconds. (a) The Au/$CePO_4$ nanocomposites, pure Au, and pure $CePO_4$ at 0.709 V. (b) $CePO_4$ and (c) $AlPO_4$ at different applied potentials.

2.3.5. Estimation of Grain Sizes

X-ray diffraction (XRD) patterns of the Au thin film and Au/$CePO_4$ nanocomposites are presented in Fig. 2-5. The Au peaks were identified as crystalline Au (JCPDS 04-0784). The grain sizes were calculated by fitting peaks and obtained as 42.90 nm, 28.70 nm, 9.1 nm, and 6.85 nm, for pure Au and the Au/$CePO_4$ nanocomposites with various deposition powers of 20 W, 40 W and 60 W, respectively. The higher deposition power of $CePO_4$ target leads to more intensive collisions before arriving ITO glass, resulting in the smaller grain sizes of Au. From the XRD patterns, it is also demonstrated that the nanostructures of the Au/$CePO_4$ are composed of crystalline Au and amorphous $CePO_4$.

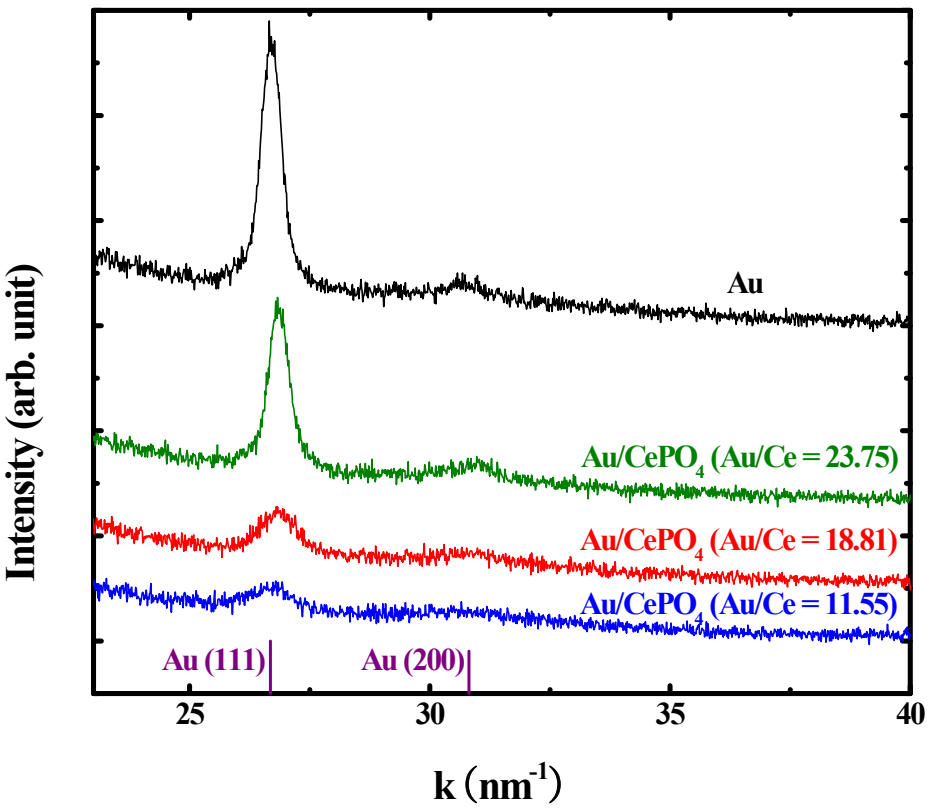

Fig. 2-5. (Color) X-ray diffraction (XRD) patterns of the Au thin film and the Au/$CePO_4$ nanocomposites. The Au peaks were identified as crystalline Au (JCPDS 04-0784).

2.4 Conclusions

The various ratios of Au/$CePO_4$ nanocomposites were prepared by co-sputtering, and oxygen reduction activity which exhibited “electronic effect” was investigated. Despite the negligible activity of pure $CePO_4$ and relatively low activity of pure Au, interestingly, the composite showed enhanced ORR activity through the 4-electron reduction process. This synergetic effect was the best for the Au/Ce = 18.81 nanocomposite with the largest ESA and lowest binding energy. The H_2O_2 reduction activity of $CePO_4$ also was proposed as one of the reasons for enhancement. A new catalyst for ORR with lower noble metal portion was developed through our approach, which showed comparable activity to Pt, and the mechanisms contributed to improved catalytic activity were revealed.

2.5 References

1. J. K. Norskov, J. Rossmeisl, A. Logadottir, and L. Lindqvist, "Origin of the Overpotential for Oxygen Reduction at a Fuel-Cell Cathode," *J. Phys. Chem. B* **108**, 17886 (2004).
2. H. Lin, W. Tang, A. Kleiman-Shwarsctein, and E. W. McFarland, "Oxygen Electroreduction on Gold-Cobalt Oxide Binary Nanocluster Catalysts," *J. Electrochem. Soc.* **155**, B200 (2008).
3. D. A. Slanac, A. Lie, J. A. Paulson, K. J. Stevenson, and K. P. Johnston, "Bifunctional Catalysts for Alkaline Oxygen Reduction Reaction via Promotion of Ligand and Ensemble Effects at Ag/MnO_x Nanodomains," *J. Phys. Chem. C* **116**, 11032 (2012).
4. D. S. Gatewood, D. E. Ramaker, K. Sasaki, and K. E. Swider-Lyonsa, "Support Effects on Water Activation and Oxygen Reduction over Au/SnO_x Electrocatalysts Observed with X-Ray Absorption Spectroscopy," *J. Electrochem. Soc.* **155**, B834 (2008).
5. J. Kim and A. A. Gewirth, "Mechanism of Oxygen Electroreduction on Gold Surfaces in Basic Media," *J. Phys. Chem. B* **110**, 6 (2006).
6. S. Strbac and R. R. Adzic, "The Influence of OH^- Chemisorption on the Catalytic Properties of Gold Single Crystal Surfaces for Oxygen Reduction in Alkaline Solutions," *J. Electroanal. Chem.* **403**, 169 (1996).
7. R. R. Adzic, N. M. Markovic, and V. B. Vesovic, "Structural effects in

electrocatalysis oxygen reduction on the Au (100) single crystal electrode," *J. Electroanal. Chem.* **165**, 105 (1984).

8. N. M. Markovic, R. R. Adzic, and V. B. Vesovic, "Structural effects in electrocatalysis oxygen reduction on the gold single crystal electrodes with (110) and (111) orientations," *J. Electroanal. Chem.* **165**, 121 (1984).
9. J. Hernandez, J. Solla-Gullon, and E. Herrero, "Gold nanoparticles synthesized in a water-in-oil microemulsion: electrochemical characterization and effect of the surface structure on the oxygen reduction reaction," *J. Electroanal. Chem.* **574**, 185 (2004).
10. J. Bockris and A. Reddy, *Modern Electrochemistry*, Plenum Press, 1970.
11. I. M. Kolthoff and C. S. Miller, "The Reduction of Oxygen at the Dropping Mercury Electrode," *J. Am. Chem. Soc.* **63**, 1013 (1941).
12. B. H. Erne, F. Ozanam, and J. N. Chazalviel, "The Mechanism of Hydrogen Gas Evolution on GaAs Cathodes Elucidated by In Situ Infrared Spectroscopy," *J. Phys. Chem. B* **103**, 2948 (1999).
13. W. P. Zhou, A. Lewera, R. Larsen, R. I. Masel, P. S. Bagus, and A. Wieckowski, "Size Effects in Electronic and Catalytic Properties of Unsupported Palladium Nanoparticles in Electrooxidation of Formic Acid," *J. Phys. Chem. B* **110**, 13393 (2006).
14. B. Hammer and J. K. Norskov, "Theoretical Surface Science and catalysis," *Adv. Catal.* **45**, 71 (2000).
15. Y. Park, B. Lee, C. Kim, J. Kim, S. Nam, Y. Oh, and B. Park, "Modification of

Gold Catalysis with Aluminum Phosphate for Oxygen-Reduction Reaction," *J. Phys. Chem. C* **114**, 3688 (2010).

16. W. Chen, J. Kim, S. Sun, and S. Chen, "Electrocatalytic Reduction of Oxygen by FePt Alloy Nanoparticles," *J. Phys. Chem. C* **112**, 3891 (2008).

Appendix

A.1. List of Publications and Presentations

A.1.1 List of Publications

1. **"Facile Synthesis of Porous-Carbon/$LiFePO_4$ Nanocomposites"**

   Sungun Wi, Seunghoon Nam, Yuhong Oh, Jongmin Kim, Hongsik Choi, Saeromi Hong, **Sujin Byun**, Suji Kang, Dong Joo Choi, Key-one Ahn, Young-Ho Kim, * and Byungwoo Park*

   J. Nanopart. Res. (2013).

2. **"Electronic Transport and Carrier Concentration in Conductive ZnO:Ga Thin Films"**

   Changwoo Nahm, Sungjin Shin, Woojin Lee, Jae Ik Kim, Dae-Ryong Jung, Jongmin Kim, Seunghoon Nam, **Sujin Byun**, and Byungwoo Park*

   Curr. Appl. Phys. **13**, 415 (2013).

3. **"Photoluminescence Enhancement in CdS Quantum Dots by Thermal Annealing"**

   Jae Ik Kim, Jongmin Kim, Junhee Lee, Dae-Ryong Jung, Hoechang Kim, Hongsik Choi, Sungjun Lee, **Sujin Byun**, Suji Kang, and Byungwoo Park*

   Nanoscale Res. Lett. **7**, 482 (2012).

4. **"The Role of Carbon Incorporation in SnO_2 Nanoparticles for Li Rechargeable Batteries"**

Seunghoon Nam, Sungsoo Kim, Sungun Wi, Hongsik Choi, **Sujin Byun**, Soon-Mi Choi, Sang-Im Yoo, Kyu Tae Lee,* and Byungwoo Park*

J. Power Sources **211**, 154 (2012).

5. **"Surface-Plasmon-Coupled Photoluminescence from CdS Nanoparticles with Au Films"**

Jae Ik Kim, Dae-Ryong Jung, Jongmin Kim, Changwoo Nahm, **Sujin Byun**, Sungjun Lee, and Byungwoo Park*

Solid State Commun. **152**, 1767 (2012).

6. **"$Pt/AlPO_4$ Nanocomposite Thin-Film Electrodes for Ethanol Electrooxidation"**

Yuhong Oh, Joonhyeon Kang, Seunghoon Nam, **Sujin Byun**, and Byungwoo Park*

Mater. Chem. Phys. **135**, 188 (2012).

7. **"Methanol Oxidation in Nanostructured Platinum/Cerium-Phosphate Thin Films"**

Jungjin Park, Yuhong Oh, Yejun Park, Seunghoon Nam, Joonhee Moon, Joonhyeon Kang, Dae-Ryong Jung, **Sujin Byun**, and Byungwoo Park*

Curr. Appl. Phys. **11**, S2 (2011).

A.1.2. List of Presentations (International)

1. **"Oxygen Reduction on Gold/Cerium Phosphate Electrocatalyst for Alkaline Fuel Cells"**

   Sujin Byun, Joonhyeon Kang, Yuhong Oh, Suji Kang, and Byungwoo Park

   The 13th Korea - Japan Student Symposium (Seoul National University - Tohoku University), Seoul, Korea, November 7-9, 2012. **[Oral by S. Byun].**

2. **"Correlation between Catalytic Activity for Methanol Dehydrogenation and Surface Electronic Structure of Platinum"**

   Joonhyeon Kang, **Sujin Byun**, Yuhong Oh, Seunghoon Nam, Suji Kang, and Byungwoo Park

   Materials Research Society (MRS) Fall Meeting, Boston, MA, November 2012.

3. **"The Role of Carbon Incorporation in SnO_2 Nanoparticles for Li Rechargeable Batteries"**

   Seunghoon Nam, Sungsoo Kim, Sungun Wi, Hongsik Choi, **Sujin Byun**, and Byungwoo Park

   Materials Research Society (MRS) Fall Meeting, Boston, MA, November 2012.

국문 초록

최근 친환경적인 에너지 자원의 필요성이 대두됨에 따라, 연료 전지는 신 에너지변환 시스템으로써 많은 관심을 받고 있다. 연료전지는 전기화학적 원리를 이용하여 화학 에너지를 직접 전기 에너지로 변환 시키며 에너지 밀도가 높고 적용범위가 다양한 것이 장점이다. 비록 연료전지 분야에서 많은 연구들이 진행되어 왔으나, 백금 촉매의 가격문제, 백금을 제외한 다른 소재에서의 우수하지 못한 촉매활성, 그리고 촉매반응에 관한 이해 등의 문제들이 과제로 남아 있다. 이 학위 논문에서는 백금을 포함하지 않은, 금과 세륨 인산화물의 조합으로 향상된 촉매 활성을 발현시키고자 하였다.

우선, 1 장에서는 연료전지를 소개하고, 전기화학 촉매의 이해를 위하여 촉매와 반응물간의 전자 공유 및 혼성에 기인한 화학적 흡착에 대하여 살펴보았다. 나아가 중간 반응물, 반응 경로, 활성화 에너지 간의 관계에 대하여서도 알아 볼 것이다. 또한, 화학적 흡착세기와 *d*-band orbital 의 변화 그리고 산소 환원 반응의 활성 비교를 보여줌으로써, 촉매 활성에 영향을 미칠 수 있는 여러 요인들을 확인할 것이다.

2 장에서는 Au 과 $CePO_4$ 을 동시에 증착하여 나노 구조를 가진 복합체를 형성하고, 나노 복합체의 산소 환원촉매로서의 역할을 염기성 전해질 내에서 살펴보았다. Au 촉매는 산소 환원 시, 불완전한 반응인 2-electron path 로 HO_2^-를 생성하였으나, Au/$CePO_4$ 나노 복합체는 같은 전위범위 내에서도 4 개의 전자를 받아 OH^-이온으로 산소 환원반응을 완료시키는 특성을 보였다. 이러한 촉매능력의 향상은 Au 가 주변의 $CePO_4$ 와의 상호작용으로 인해 전자 구조가 변하였기 때문이며, 이것은 x-ray photoelectron spectroscopy 를 통해 Au 4*f* peak 의 이동으로 확인하였다. 또한 $CePO_4$ 의 HO_2^-

에 대한 촉매적 활성도 추가적 산소 환원반응에 기여하였으며 이는 Chronoamperometry 를 이용해 확인할 수 있었다.

주요어: 금, 세륨 인산화물, 전기화학적 촉매, 산소 환원 반응, 전기적 상호 영향, 염기성 연료전지, 나노 복합체

학번: 2011-22864